

## HD 1397b: a transiting warm giant planet orbiting a $V = 7.8$ mag sub-giant star discovered by TESS

RAFAEL BRAHM,<sup>1,2,3</sup> NÉSTOR ESPINOZA,<sup>4,\*</sup> ANDRÉS JORDÁN,<sup>2,3</sup> THOMAS HENNING,<sup>4</sup> PAULA SARKIS,<sup>4</sup> MATÍAS I. JONES,<sup>5</sup>  
MATÍAS R. DÍAZ,<sup>6</sup> JAMES S. JENKINS,<sup>6</sup> LEONARDO VANZI,<sup>1</sup> ABNER ZAPATA,<sup>1</sup> CRISTOBAL PETROVICH,<sup>7</sup>  
DIANA KOSSAKOWSKI,<sup>4</sup> MARKUS RABUS,<sup>2,4</sup> AND PASCAL TORRES<sup>2</sup>

<sup>1</sup>Center of Astro-Engineering UC, Pontificia Universidad Católica de Chile, Av. Vicuña Mackenna 4860, 7820436 Macul, Santiago, Chile

<sup>2</sup>Instituto de Astrofísica, Pontificia Universidad Católica de Chile, Av. Vicuña Mackenna 4860, Macul, Santiago, Chile

<sup>3</sup>Millennium Institute for Astrophysics, Chile

<sup>4</sup>Max-Planck-Institut für Astronomie, Königstuhl 17, Heidelberg 69117, Germany

<sup>5</sup>European Southern Observatory, Casilla 19001, Santiago, Chile

<sup>6</sup>Departamento de Astronomía, Universidad de Chile, Camino El Observatorio 1515, Las Condes, Santiago, Chile

<sup>7</sup>Canadian Institute for Theoretical Astrophysics, University of Toronto, 60 St George Street, ON M5S 3H8, Canada

Submitted to AAS Journals

### ABSTRACT

We report the discovery of a transiting planet first identified as a candidate in Sector 1 of the Transiting Exoplanet Survey Satellite (*TESS*), and then confirmed with precision radial velocities. HD 1397b has a mass of  $M_P = 0.335^{+0.018}_{-0.018} M_J$ , a radius of  $R_P = 1.021^{+0.015}_{-0.014} R_J$ , and orbits its bright host star ( $V = 7.8$  mag) with an orbital period of  $11.53508 \pm 0.00057$  d, on a moderately eccentric orbit ( $e = 0.210 \pm 0.038$ ). With a mass of  $M_\star = 1.284^{+0.020}_{-0.016} M_\odot$ , a radius of  $R_\star = 2.314^{+0.049}_{-0.042} R_\odot$ , and an age of  $4.7 \pm 0.2$  Gyr, the solar metallicity host star has already departed from the main sequence. We find evidence in the radial velocity measurements for a long term acceleration, and a  $P \approx 18$  d periodic signal that we attribute to rotational modulation by stellar activity. The HD 1397 system is among the brightest systems currently known to host a transiting planet, which will make it possible to perform detailed follow-up observations in order to characterize the properties of giant planets orbiting evolved stars.

*Keywords:* editorials, notices — miscellaneous — catalogs — surveys

### 1. INTRODUCTION

Throughout the past two decades, several ground-based, small-aperture, wide-field photometric surveys (e.g. Bakos et al. 2004; Pollacco et al. 2006; Pepper et al. 2007; Bakos et al. 2013; Talens et al. 2017) have efficiently detected and characterized the population of short-period transiting giant planets orbiting bright stars across the whole sky. These discoveries have triggered significant advances in the study of the formation and evolution of planetary systems, and have been targets of detailed follow-up observations to study their orbital configurations (e.g. Triaud et al. 2010; Zhou et al. 2015; Esposito et al. 2017) and atmospheric composi-

tions (e.g. Spake et al. 2018; Chen et al. 2018; Jensen et al. 2018). Nonetheless, due to strong observational biases produced by the Earth’s atmosphere and the limited duty cycle of ground-based facilities, there is still a region of parameter space of giant planets that is vastly unexplored. Specifically, transiting systems of giant planets having orbital periods longer than  $\approx 10$  d have scarcely been detected from the ground (Kovács et al. 2010; Lendl et al. 2014; Hellier et al. 2017; Brahm et al. 2016). Additionally, due to the decrease in transit depth, we only have a handful of giant planets orbiting stars that have recently left the main sequence with radii larger than  $2.2 R_\odot$  (Hartman et al. 2012; Smith et al. 2013; Rabus et al. 2016; Bento et al. 2018). The characterization of transiting giant planets having periods longer than 10 d, and/or orbiting evolved stars is important for understanding the processes that govern the formation, evolution and fate of giant planets. The

Corresponding author: Rafael Brahm  
rbrahm@astro.puc.cl

\* Bernoulli fellow; Gruber fellow

detailed study of the distribution of eccentricities and spin-orbit angles of giant planets orbiting beyond 0.1 AU can be used to constrain migration theories (Dong et al. 2014; Petrovich & Tremaine 2016; Anderson & Lai 2017), while the characterization of planets orbiting giant and sub-giant stars can be used to infer the nature of the inflation mechanism of hot Jupiters (Lopez & Fortney 2016), characterizing tidal interactions (e.g. Villaver & Livio 2009), and understanding the Lithium excess observed in some evolved stars (e.g. Aguilera-Gómez et al. 2016). Very recently, the *K2* mission (Howell et al. 2014) started to contribute to the detection of giant planets orbiting bright stars having  $P > 10$  d (e.g. Shporer et al. 2017; Brahm et al. 2018; Yu et al. 2018; Jordán et al. 2018), and giant planets orbiting evolved stars (e.g. Grunblatt et al. 2017; Jones et al. 2018). While not being its primary scientific driver, the *TESS* mission (Ricker et al. 2015) is expected to discover several hundreds giant planets orbiting bright stars ( $V < 12$  mag), having periods longer than 10 d, and/or orbiting evolved stars (Barclay et al. 2018). Therefore, it is expected that *TESS* will yield for the first time a statistically significant sample for these kind of objects that will be useful for constraining theories of planetary formation and evolution. Interestingly, the first confirmed giant planet from *TESS* orbits a slightly evolved star (Wang et al. 2018).

In this study we present the discovery of HD 1397b, the first giant planet discovered by the *TESS* mission with an orbital period longer than 10 days. In addition to its long period, the host star is a bright ( $V = 7.8$ ) sub-giant star, making this a very interesting system for further study.

## 2. OBSERVATIONS

### 2.1. *TESS*

Between 2018 July 25 and 2018 August 22, the *TESS* mission observed HD 1397 (TIC 394137592, TOI00120.01) with its Camera 3, during the monitoring of the first *TESS* sector. Observations were performed with a cadence of 2 minutes. Photometric data of HD 1397 were analyzed with the Science Processing Operations Center (SPOC) pipeline, which is a modified version of the pipeline used for the NASA Kepler mission (Jenkins et al., in prep). This light curve was released to the community on September 15 of 2018 as an alert. The alert did not report warning flags that could be associated with false positive scenarios. In particular, there is no statistical difference between transit depths, and there are no significant centroid offsets of the PSF during the transits.

The *TESS* light curve of HD 1397 is presented in Figure 1, after removing flagged data points, and shows the presence of two clear, moderately deep ( $\approx 2500$  ppm) transits separated by  $\approx 11.5$  days. We masked out the in-transit points and ran a Gaussian process (GP) regression with the quasi-periodic kernel introduced in (Foreman-Mackey et al. 2017) in the data, in order to both detrend the lightcurve and predict the in-transit trends, allowing for a photometric jitter term in this fit. The best-fit GP is shown in Figure 2, and this GP was divided into our data in order to compute a detrended lightcurve, propagating the prediction errors into the photometric errors. As can be seen, the in-transit prediction shows a decreasing slope on the second transit, whereas in the first transit the GP prediction is relatively flat.

### 2.2. High resolution spectroscopy

We started the radial velocity follow-up of HD 1397 a couple of hours after the first alerts of *TESS* Sector 1 were made public. We obtained two spectra with the HARPS spectrograph (Mayor et al. 2003) installed at the ESO 3.6m telescope at La Silla Observatory on two consecutive nights. We adopted an exposure time of 300s and pointed the comparison fiber to the background sky. Additionally, we obtained 35 spectra with the FIDEOS spectrograph (Vanzi et al. 2018) installed at the 1-m telescope on the same observatory. FIDEOS observations were obtained on six consecutive nights. For these observations we adopted an exposure time of 600 s and the comparison fiber was used to trace the instrumental radial velocity drift by observing a ThAr lamp. The HARPS and FIDEOS data were processed with the CERES package (Brahm et al. 2017a), which automatically performs optimal spectral extraction from the raw images, wavelength calibration, instrumental drift correction, and the computation of the radial velocities and bisector spans. The radial velocities were computed with the cross-correlation technique by using a binary mask with a set of lines compatible with a G2-type star. These radial velocities were consistent with an absence of large variations that could have been produced by a stellar companion, and they hinted the presence of a relatively low amplitude signal ( $\approx 30$  m s $^{-1}$ ) in phase with the photometric ephemeris. Additionally, no secondary peaks were identified in the cross-correlation function that could have indicated the presence of possible background diluted eclipsing binaries.

We then proceeded to perform intensive radial velocity monitoring of HD 1397 with the FEROS spectrograph installed at the MPG 2.2m telescope at La Silla Observatory (Kaufer et al. 1999). Two additional HARPS

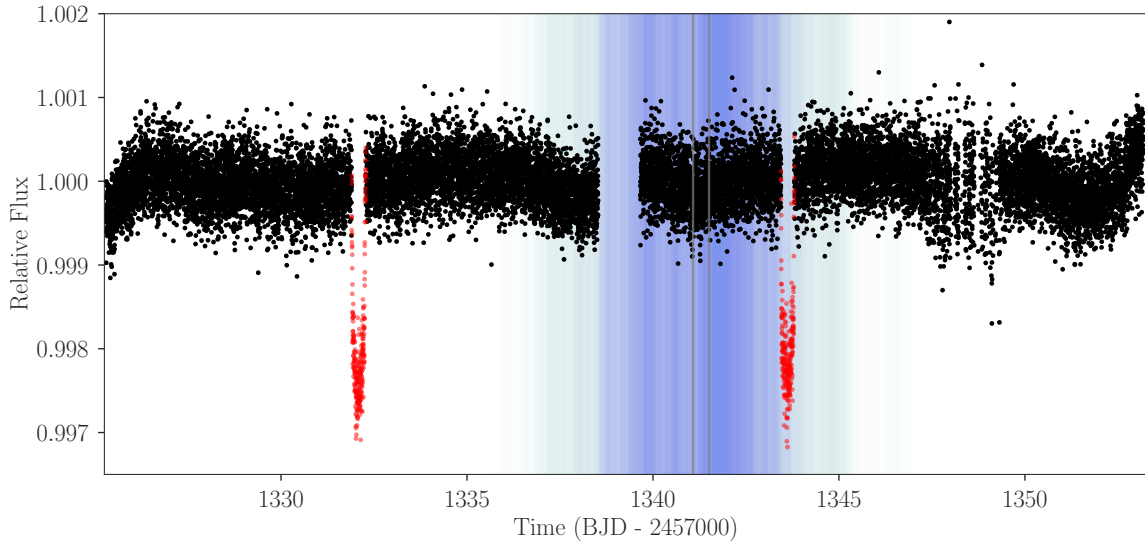


**Figure 1.** *TESS* 2 minute cadence light curve for HD 1397. The two transits are plotted in red. The blue region represents the probability distribution for a transit produced by a planet having orbital parameters equal to those determined for the second radial velocity signal (see Section 3.3)

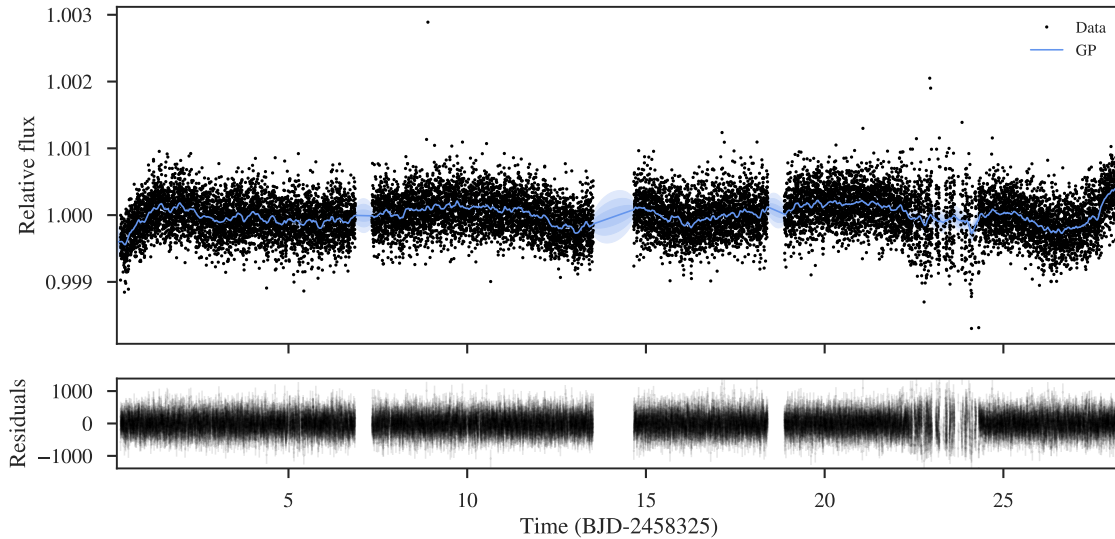


**Figure 2.** *TESS* lightcurve with the transits masked out and a quasi-periodic kernel fitted to the data. This kernel was used to detrend the lightcurve and, especially, remove predicted long term trends in-transit.

spectra were acquired during this period. FEROS observations were performed with the simultaneous calibration mode and the adopted exposure time was of 300s. We obtained 52 spectra on time span of 40 nights. FEROS data were also processed with the CERES package. In addition to the bisector span measurements, the S-index activity indicator was computed for each spectrum as described in Jenkins et al. (2008); Jones et al. (2017). HD 1397 presents significant and time variable chromospheric emission as gauged from the Ca II H & K lines of the FEROS and HARPS spectra. The radial ve-

locities, bisector spans, and S-indexes obtained with the three instruments are presented in Table 3. The velocities are plotted as a function of time in Figure 3. The FEROS velocities confirmed the presence of the periodic signal initially hinted by FIDEOS, and also allowed the detection of a long term radial velocity trend. Additionally, no significant correlation was found between the radial velocity and bisector span measurements at the 95% level of confidence (see Figure 4) A greater correlation was found between the S-index and the radial velocity measurements but it was still not significant at

the 95% level of confidence. The relation between the radial velocity, bisector span, and activity measurements are further explored in Section 3.2.

### 3. ANALYSIS

#### 3.1. *Properties of the host star*

We analyzed the co-added FEROS spectra to obtain the atmospheric parameters of HD 1397. We used the ZASPE code (Brahm et al. 2017b), which compares the observed spectrum to a grid of synthetic models generated from the ATLAS9 model atmospheres (Castelli & Kurucz 2004). The search for the optimal model is performed only in the spectral zones that are most sensitive to changes in the atmospheric parameters. The errors in the derived parameters are obtained from Monte Carlo simulations where the depth of the spectral lines of the synthetic models are perturbed in order to properly account for the systematic model mismatch as the main source of the error budget. We obtained that HD 1397 has an effective temperature of  $T_{\text{eff}} = 5479 \pm 50$  K, a surface gravity of  $\log g = 3.816 \pm 0.006$  dex, a metallicity of  $[\text{Fe}/\text{H}] = +0.04 \pm 0.04$  dex, and a projected rotational velocity of  $v \sin i = 4.0 \pm 0.3$  m s<sup>-1</sup>.

In order to estimate the radius of HD 1397, we followed the same procedure presented in Brahm et al. (2018). We interpolated the stellar models presented in Baraffe et al. (2015) to generate a synthetic spectral energy distribution (SED) consistent with the atmospheric parameters found for HD 1397. We then generated synthetic magnitudes from the SED by integrating it in different spectral zones, weighted by the corresponding transmission functions of the passband filters presented in Table 1. These synthetic magnitudes were used to estimate the stellar radius ( $R_{\star}$ ) and the extinction factor ( $A_V$ ) by comparing them to the publicly reported magnitudes after converting them to absolute magnitudes using the distance obtained from the GAIA DR2 parallax measurement (Gaia Collaboration et al. 2016, 2018). We obtained the posterior distribution for  $R_{\star}$  and  $A_V$  by using the emcee Python package (Foreman-Mackey et al. 2013). In order to consider the uncertainty in the atmospheric parameters, we repeated this process for different values of  $T_{\text{eff}}$  sampled from a Gaussian distribution with the parameters obtained with the ZASPE analysis. We find that HD 1397 has a radius of  $R_{\star} = 2.314^{+0.049}_{-0.042} R_{\odot}$ , and an extinction factor consistent with  $A_V = 0$ .

Finally, we estimated the mass and evolutionary stage of HD 1397 by comparing its effective temperature and radius to those predicted by stellar evolutionary models. Specifically, we used the Yonsei-Yale evolutionary models (Yi et al. 2001) which were interpolated to the

metallicity derived for HD 1397. We used the emcee package to compute the posterior distributions for the stellar mass and age. We find that HD 1397 has a mass of  $M_{\star} = 1.284^{+0.020}_{-0.016} M_{\odot}$ , and an age of  $4.7 \pm 0.2$  Gyr. The stellar parameters obtained for HD 1397 are presented in Table 1 along with its observed properties.

#### 3.2. *Radial Velocities*

Motivated by the slight but not significant correlation between the radial velocities and the activity indicators, and also due to the presence of time correlated residuals in some preliminary modeling of the radial velocities, we proceeded to analyze all the available time series. We computed the generalized Lomb-Scargle periodograms (GLS, Zechmeister & Kürster 2009) for the non-detrended *TESS* photometry, radial velocities, bisector span measurements, and S-index values. For the *TESS* photometry we masked out the two transits. The significance of the peaks in the periodograms was evaluated by performing a bootstrap of each time series. The four periodograms are plotted in Figure 5. The bottom panel of Figure 5 shows that the radial velocity measurements are able by themselves to recover with high significance the 11.5 day periodic signal of the planet candidate observed in the *TESS* transits. Additionally, there are no peaks in the periodograms of the bisector spans and S-index associated to that particular period. Interestingly, the periodogram of the *TESS* photometry presents a peak close to the orbital period of the system. If the associated signal is not an artifact of the SPOC pipeline, given the large ratio between the radii of the star and the planet, the source of this periodic variation could be associated to changes on the star (e.g. ellipsoidal variations, Welsh et al. 2010) rather than phase curve variations.

Figure 5 shows also the presence of a secondary wide significant peak at  $\approx 18.5$  days in the radial velocity periodogram. This periodic signal is also present with high significance in the S-index time series, and marginally present in the bisector span measurements. These signals can be associated to the rotational modulation of active regions on the stellar surface. Given the relatively short time span of our spectroscopic observations (2 months), the active regions on the star, such as spots, faculae and/or plagues could have remain stable producing a coherent signal (Hussain 2002). If the rotation period of HD 1397 is of  $\approx 18.5$  d, by using the estimated radius of  $R_{\star} = 2.314^{+0.049}_{-0.042} R_{\odot}$ , we predict a rotational velocity at the surface of the star of  $\approx 6.3$  km s<sup>-1</sup>, which if compared with the  $v \sin i$  value estimated from our spectroscopic analysis would imply a miss-alignment an-

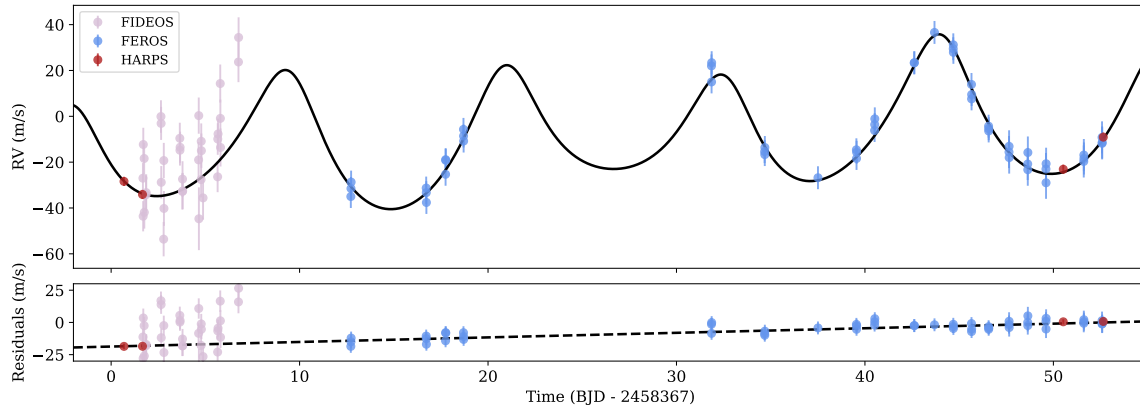


**Figure 3.** The top panel presents the radial velocity (RV) curve for HD 1397 obtained with HARPS (red), FIDEOS (pink), and FEROS (blue). The black line corresponds to the Keplerian model with the posterior parameters found in Section 3.3. The bottom panel shows the residuals without considering the radial velocity trend.

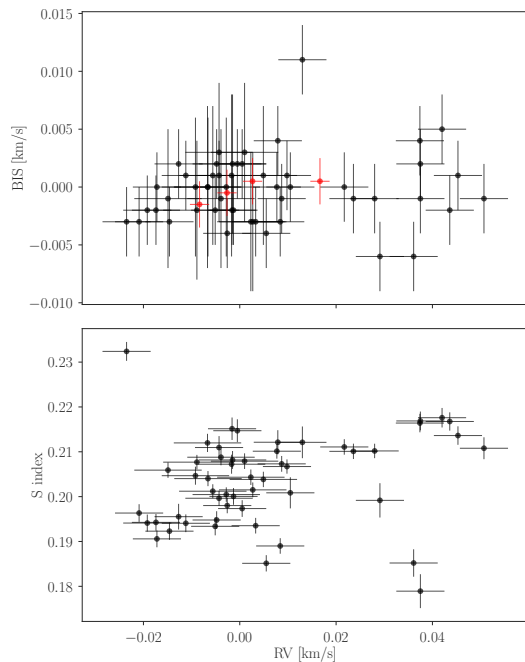


**Figure 4.** Top panel: Radial velocity – bisector span scatter plot for the FEROS (black) and HARPS (red) observations of HD 1397. No correlation is observed. Bottom panel: Radial velocity – S-index scatter plot for the FEROS observations. While the correlation value is larger in this case, it is still not significant at the 95% confidence level.

gle of  $\approx 60$  degrees between the spin of the star and the orbit of HD 1397b.

### 3.3. Global Modeling

The global modelling of the transit and radial velocities was performed with a new algorithm that will be detailed in another publication (Espinoza et al., in prep). In brief, the algorithm is similar to *exonailer* (Espinoza et al. 2016) with the main difference that in-

stead of *emcee* (Foreman-Mackey et al. 2013), the new algorithm uses MultiNest (Feroz et al. 2009) via the PyMultiNest package (Buchner et al. 2014) in order to both perform posterior sampling and model comparison directly using model evidences. The transits are modelled using *batman* (Kreidberg 2015), and the radial velocities modelled using *radvel* (Fulton et al. 2018). For limb-darkening, we use a quadratic law with the uninformative sampling scheme of Kipping (2013). This enhanced algorithm in turn also has the possibility to include dilution factors, and variable mean fluxes for different photometric instruments, as well as the possibility of fitting multiplanetary systems for both transits and radial velocities simultaneously. Several types of trends as a function of time can also be modelled in the radial velocities including linear and quadratic trends. For these latter trends, the fitting parameters in our approach are the terms that accompany the linear and quadratic terms, along with a parameter  $T_{rv,0}$ , which is the time at which this linear trend crosses the line of zero radial velocity once the planetary signals and instrumental offsets of the radial-velocities are removed. This parametrization is made such that a convenient prior can be defined for this parameter.

We considered several fits for our data, which showed not only an evident linear trend, but also an extra periodic signal that appeared in the residuals once we subtracted a fit considering only the transiting exoplanet and said linear trend, hinting at a period of about 18 days, in line with the observed periodograms shown in Figure 5. We thus fitted an extra keplerian signal to the radial-velocities in our joint analysis with a large prior around this period, which in turn gave a larger evidence for this model later ( $\ln Z > 5$ , i.e., a Bayes factor assuming both models are equally likely of  $\sim 150$  in favor of the model containing the extra signal). Interestingly,

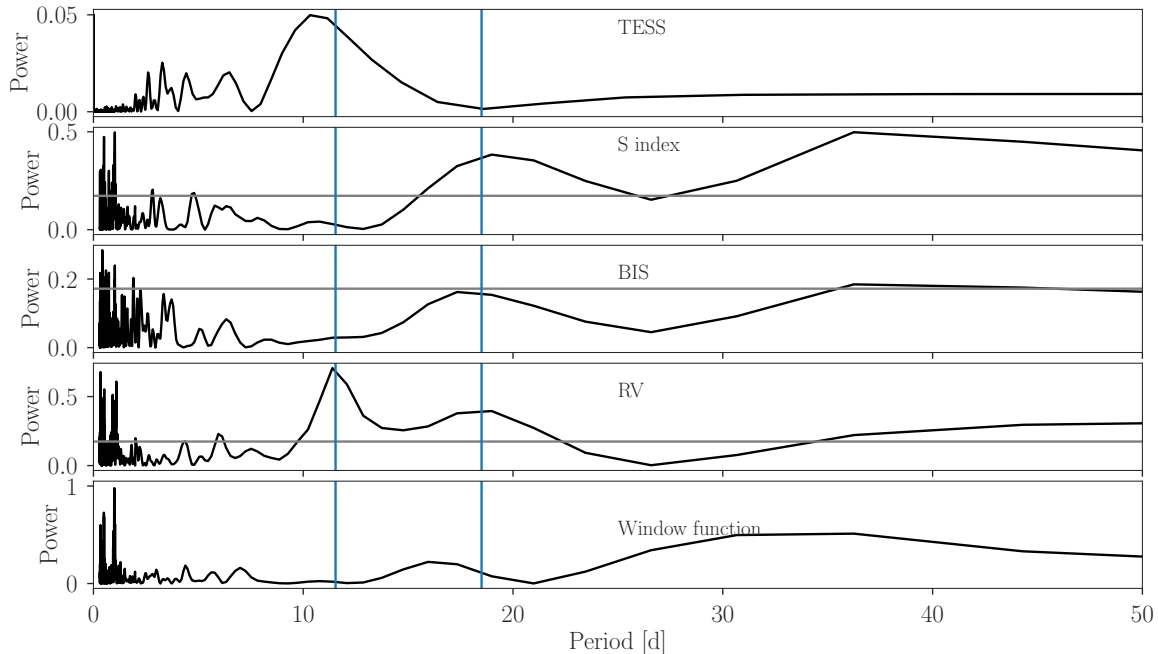


**Figure 5.** GLS power spectra for the *TESS* photometry, S-index, bisector spans, radial velocities of HD 1397 and window function (black lines from top to bottom). The gray lines represent the 1% significance limits based on bootstrap simulations. The radial velocities present a primary peak at  $\approx 11.5$  days which is consistent with the orbital period of the planetary candidate obtained from the *TESS* photometry. There is a secondary peak in the periodogram of the radial velocities at  $\approx 18.5$  days, which can be associated with the rotational modulation of activity regions in the surface of the star.

the posterior parameters for the secondary signal imply that if it is due to another transiting planet, there is a high probability that the transit would have occurred during the the gap in the *TESS* light curve produced during the downlink of the data from the satellite (Figure 1). However, considering the signals observed in the periodograms for other activity indicators (see Figure 5), we consider it more likely that this signal is generated by stellar activity. The parameters obtained from the global modeling are presented in Table 2.

By combining the results of the global analysis with the physical parameters derived for the stellar host, we find that HD 1397b has a Saturn-like mass of  $M_P = 0.335^{+0.018}_{-0.018} M_J$ , but a radius that is more similar to that of Jupiter ( $R_P = 1.021^{+0.015}_{-0.014} R_J$ ). HD 1397b has a semi-major axis of  $a = 0.10866^{+0.00037}_{-0.00045}$  AU, which coupled to its orbital eccentricity results in a distance to the star at periastris of  $0.08306 \pm 0.00003$  AU. This orbital configuration also results in an averaged equilibrium temperature for HD 1397b of  $T_{eq} = 1213 \pm 17$  K, assuming zero albedo and full energy redistribution. The derived parameters of HD 1397b are listed in Table 2.

## 4. DISCUSSION

### 4.1. Structure

the

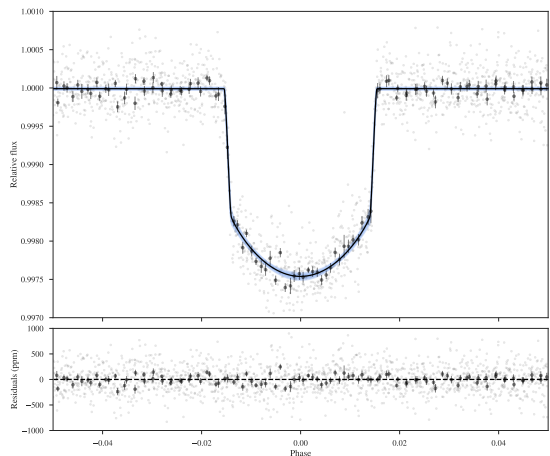


**Figure 6.** Phase folded *TESS* photometry for HD 1397. The model generated with the derived parameters of our joint modelling is plotted with a black line. The bottom panel shows the corresponding residuals.

HD 1397b adds up to the still sparse, but recently growing, population of transiting giant planets with well constrained parameters orbiting beyond 0.1 AU (see Figure 8). While located relatively far from its host star if compared to the typical population of hot Jupiters, the moderately massive stellar host ( $M_\star = 1.284^{+0.020}_{-0.016} M_\odot$ ) is responsible for producing insolation levels on

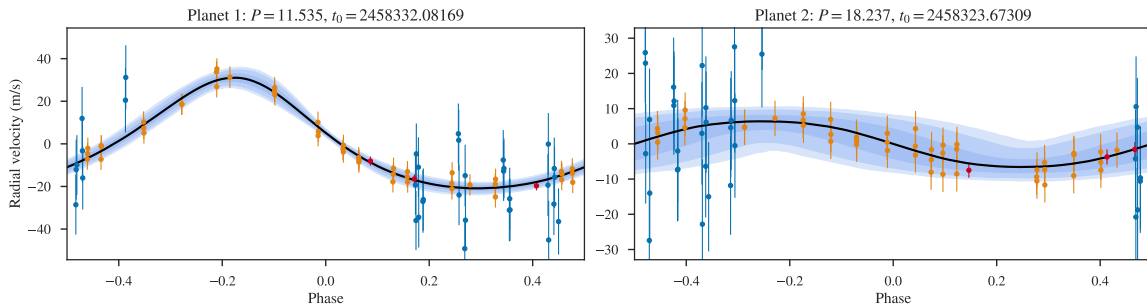


**Figure 7.** Left panel: Radial Velocities as a function of the orbital phase for HD 1397b obtained with FIDEOS (blue), FEROS (yellow) and HARPS (red). The black line represents the keplerian model generated from the posterior distributions obtained in Section 3. Right panel: same figure but for the second keplerian signal of our modeling.

HD 1397b that are high enough ( $T_{\text{eq}} = 1213 \pm 17$  K) to possibly alter the internal planetary structure (Kovács et al. 2010; Demory & Seager 2011). Therefore, in terms of structure, HD 1397b shares similar properties to other known low mass hot Jupiters, like WASP-83b (Hellier et al. 2015), HATS-21b (Bhatti et al. 2016), and WASP-160b (Lendl et al. 2018) (see Figure 9).

Regardless of its moderately high equilibrium temperature, the observed physical properties of HD 1397b are still consistent with standard structural models. Specifically, using the Fortney et al. (2007) models, we obtain that given the current stellar age, luminosity, and star-planet separation, the structure of HD 1397b requires the presence of a core of  $\approx 8.3 \pm 2.5 M_{\oplus}$  of solid material, which is consistent with the values expected in the core accretion model of planet formation (Pollack et al. 1996).

Even though, HD 1397b presents a relatively shallow transit depth, the bright host star coupled to the relatively low density of the planet, make of the HD 1397 system a well suited target for transmission spectroscopy observations (see Figure 9). Specifically, with a transmission spectroscopy metric of  $\text{TSM} = 253$ , HD 1397b would be ranked in the first quartile for atmospheric characterization as proposed by Kempton et al. (2018). HD 1397 along with HD 209458 (Henry et al. 2000) and HD 189733 (Bouchy et al. 2005) are the three brightest systems known to host transiting giant planets.

#### 4.2. Orbital Evolution

The orbital parameters of HD 1397b are well suited for studying the migration mechanism of close-in giant planets. Its current distance to the star during periastron passages is too large for producing significant migration by tidal interactions, and therefore the orbital properties should contain information about the migration history. As an important fraction of other recently discovered transiting warm Jupiters, HD 1397b presents a moderate eccentricity ( $e = 0.210 \pm 0.038$ ). Eccentricity excitation is expected to be suppressed during

the disk lifetime (Dunhill et al. 2013), and therefore the gentle disc migration mechanism is at odds with these observations. Additionally, planet-planet scattering at these short orbital distances should preferentially produce collisions between planets, rather than the excitation of eccentricities<sup>1</sup> (Petrovich et al. 2014). Eccentricities of the observed population of warm Jupiters can be enhanced by secular gravitational interactions with other exterior orbiting companions having eccentric and/or highly miss-aligned orbits (Kozai 1962; Lidov 1962; Naoz 2016). In this scenario the eccentricity and spin-orbit angle of the inner planet suffer periodic variations in timescales significantly larger than the orbital period, and when the eccentricity approaches unity, the planets experiences significant inward migration. Additionally, Dong et al. (2014) predicts that the perturber should be close enough in order to overcome the precession caused by general relativity. HD 1397b presents properties that can be associated with this last scenario of planet migration. In addition to its eccentric orbit, HD 1397b experiences an acceleration that could be associated with the presence of a massive outer companion, a scenario that can be tested with long term radial velocity monitoring. Additionally, the measurement of the miss-alignment angle between the spin of the star and the orbital plane through the observation of the Rossiter- McLaughlin effect, could further help in constraining migration mechanism. While the expected amplitude of the Rossiter-McLaughlin effect is relatively small ( $K_{RM} \approx 8 \text{ m s}^{-1}$  for an aligned orbit), the signal should be detectable by a wide range of instruments given the brightness of the host star.

It is interesting also to note that the second signal observed in the radial velocities can be probably ruled out as having a planetary origin based on stability criteria.

<sup>1</sup> More quantitatively, the collisions largely dominate as the escape velocity of the planet of  $\sim 35 \text{ km s}^{-1}$  is significantly lower than its orbital velocity of  $\sim 100 \text{ km s}^{-1}$ .

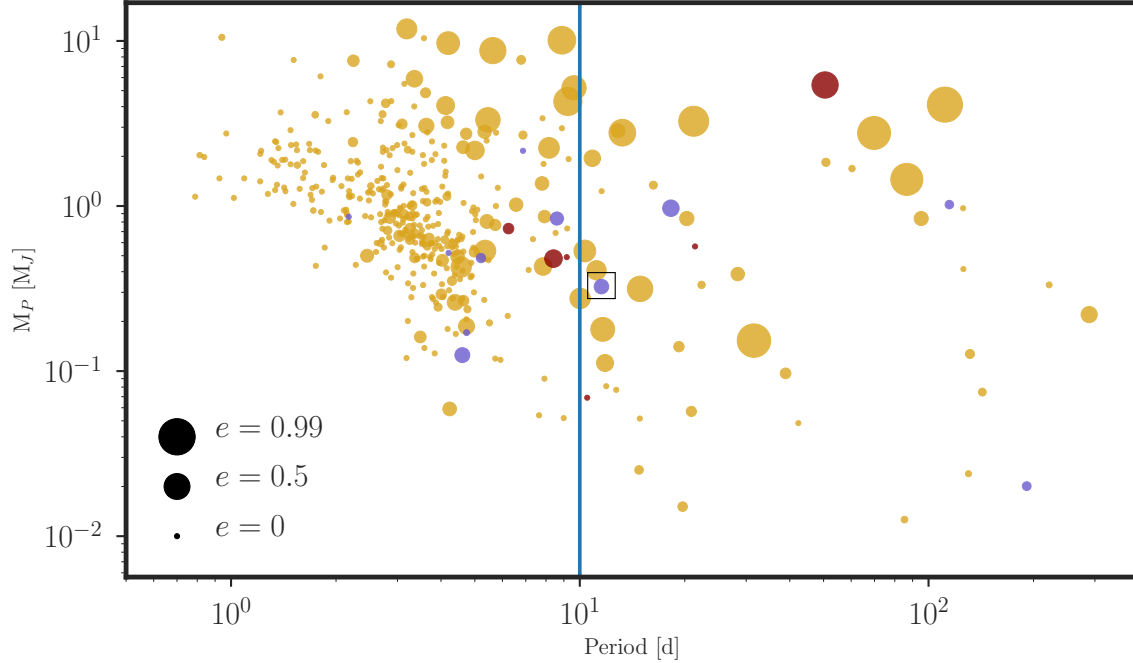


**Figure 8.** Planet mass versus orbital period scatter plot for the population of giant transiting planets with masses and radii measured with a precision of 20% or better. The size of the points scales with the orbital eccentricity and the color represents the evolutionary state of the host star (yellow: main sequence stars, purple: sub-giant stars, red: giant stars. The vertical line corresponds to the approximate division between hot and warm Jupiters (10 days). The position of HD 1397b is marked with a square.)

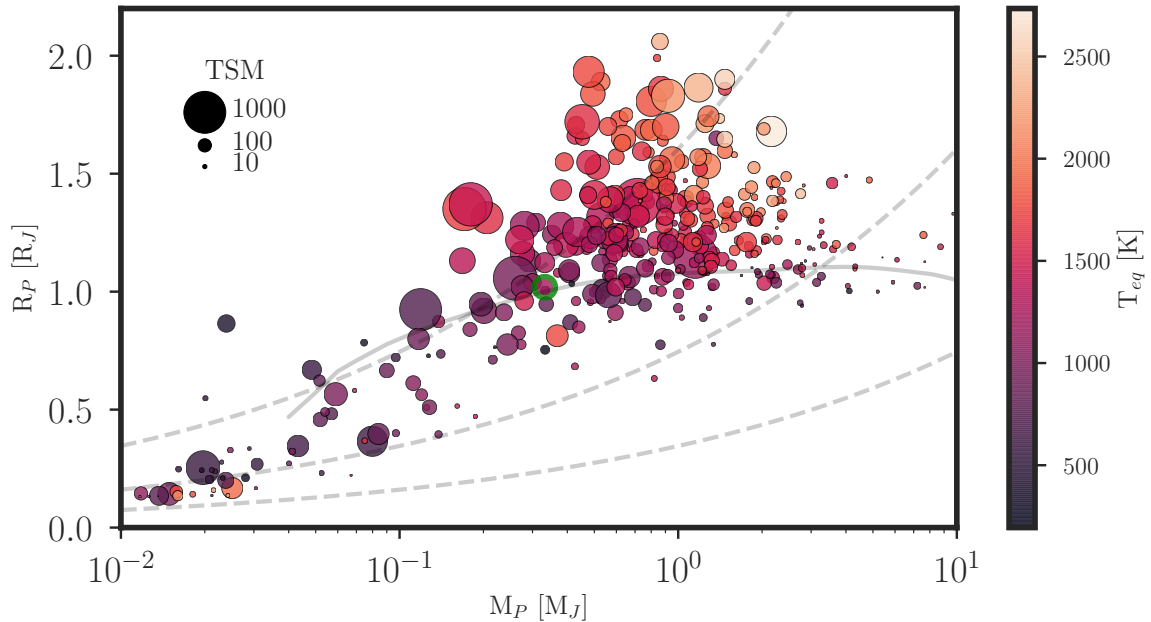


**Figure 9.** Mass – Radius diagram for the population of well characterized transiting planets. The point corresponding to HD 1397b is marked with a green contour. The color represents the equilibrium temperature of the planet, while the size scales down with the transmission spectroscopy metric as defined by [Kempton et al. \(2018\)](#). The dashed gray lines correspond to iso-density curves for  $0.3$ ,  $3$  and  $30 \text{ g cm}^{-3}$ , respectively. The solid line corresponds to the predicted radius using the models of [Fortney et al. \(2007\)](#) for a planet with a  $10 M_{\oplus}$  central core.

**Table 1.** Stellar properties of HD 1397

Parameter	Value	Reference
Names .....	HD 1397	
	TIC 394137592	TESS
	HIP 1419	HIPPARCOS
	2MASS J00174714-6621323	2MASS
	TYC 8846-638-1	TYCHO
RA .....(J2000)	00h17m47.14s	TESS
DEC .....(J2000)	-66d21m32.35s	TESS
pm <sup>RA</sup> (mas yr <sup>-1</sup> )	64.76 ± 0.05	GAIA
pm <sup>DEC</sup> (mas yr <sup>-1</sup> )	-5.06 ± 0.04	GAIA
$\pi$ .....(mas)	12.54 ± 0.03	GAIA
T .....(mag)	7.14 ± 0.03	TESS
B .....(mag)	8.47 ± 0.05	APASS
V .....(mag)	7.79 ± 0.03	APASS
J .....(mag)	6.44 ± 0.02	2MASS
H .....(mag)	6.09 ± 0.05	2MASS
K <sub>s</sub> .....(mag)	5.99 ± 0.02	2MASS
WISE1 .....(mag)	6.02 ± 0.09	WISE
WISE2 .....(mag)	5.90 ± 0.04	WISE
WISE3 .....(mag)	5.99 ± 0.02	WISE
T <sub>eff</sub> .....(K)	5479 ± 50	zaspe
log <i>g</i> .....(dex)	3.816 ± 0.006	zaspe
[Fe/H] .....(dex)	+0.04 ± 0.04	zaspe
<i>v</i> sin <i>i</i> ....(km s <sup>-1</sup> )	4.0 ± 0.3	zaspe
M <sub>*</sub> .....(M <sub>⊙</sub> )	1.28 <sup>+0.020</sup> <sub>-0.016</sub>	YY + GAIA
R <sub>*</sub> .....(R <sub>⊙</sub> )	2.314 <sup>+0.049</sup> <sub>-0.042</sub>	GAIA + this work
L <sub>*</sub> .....(L <sub>⊙</sub> )	4.32 ± 0.19	YY + GAIA
M <sub>V</sub> .....(mag)	3.30 ± 0.06	YY + GAIA
Age .....(Gyr)	4.7 ± 0.2	YY + GAIA
$\rho_*$ .....(g cm <sup>-3</sup> )	0.147 ± 0.004	YY + GAIA

For example, according to the semi-empirical criterion by [Giuppone et al. \(2013\)](#), a planet with a mass of  $0.12 M_{\text{J}}$  on a circular orbit with a period of 18.24 d, would make the system unstable as

$$1 - \left(\frac{P}{P_c}\right)^{2/3} \frac{1+e}{1-e^c} < 1.57 \left[ \left(\frac{M_P}{M_\star}\right)^{2/7} + \left(\frac{M_P^c}{M_\star}\right)^{2/7} \right]. \quad (1)$$

We caution, however, that the candidate has a period ratio of  $\approx 1.58$ , which places the planet pair near to the 5:3 mean-motion resonance, possibly allowing for islands of stability. Assessing the long-term stability of the system is beyond the scope of this work.

#### 4.3. Evolved host star

HD 1397b is a peculiar system due to the evolutionary stage of its host star. Radial velocity surveys have found that close-in giant planets are rare around giant and sub-giant stars, if compared to the the occurrence rate on main sequence stars (e.g. [Bowler et al. 2010](#); [Johnson et al. 2010](#); [Jones et al. 2014](#)). Two mechanisms have been invoked to explain this. First, the inferred stellar masses for this sample are systematically higher than those of the giant planets orbiting main sequence stars, and hence the formation of giant planets at close orbital distances or their migration from beyond the snowline could be prevented due to a shorter lifetime of the protoplanetary disc (e.g. [Currie 2009](#)). On the other hand, the scarcity of giant planets orbiting evolved stars could be also produced by the spiral decay of the orbits due to the increase in the strength of stellar tides (e.g. [Villaver & Livio 2009](#); [Schlaufman & Winn 2013](#); [Villaver et al. 2014](#)). HD 1397b joins the small group of  $\approx 10$  well characterized transiting systems of giant planets in close-in orbits around sub-giant stars (see Figure 8). An important fraction of these close-in systems, including HD 1397b, present accelerations in their radial velocity curves: Kepler-435b ([Almenara et al. 2015](#)), K2-39b ([Van Eylen et al. 2016](#)), K2-99b ([Smith et al. 2017](#)), KELT-11b ([Pepper et al. 2017](#)). While [Knutson et al. \(2014\)](#) shows that 50% of

the population of hot Jupiters orbiting main sequence stars have outer companions, the radial velocity slopes derived for this population are statistically smaller than those present in the population of close-in planets orbiting sub-giant stars. These observations indicate that the populations of close-in planets orbiting main sequence and sub-giant stars are probably distinct, where the latter have more massive and/or closer companions. In the forthcoming years, the *TESS* mission is expected to produce a statistically significant sample of close-in transiting giant planets orbiting evolved stars, which will allow to further study the origin of the low occurrence rate of this type of planetary systems.

R.B. acknowledges support from FONDECYT Postdoctoral Fellowship Project 3180246, and from the Millennium Institute of Astrophysics (MAS). A.J. acknowledges support from FONDECYT project 1171208, CONICYT project Basal AFB-170002, and by the Ministry for the Economy, Development, and Tourism’s Programa Iniciativa Científica Milenio through grant IC120009, awarded to the Millennium Institute of Astrophysics (MAS). M.R.D. is supported by CONICYT-PFCHA/Doctorado Nacional-21140646, Chile. J.S.J. acknowledges support by FONDECYT project 1161218 and partial support by BASAL CATA PFB-06. A.Z. acknowledges support by CONICYT-PFCHA/Doctorado Nacional 21170536, Chile. We acknowledge the use of *TESS* Alert data, which is currently in a beta test phase, from pipelines at the *TESS* Science Office and at the *TESS* Science Processing Operations Center. This research has made use of the Exoplanet Follow-up Observation Program website, which is operated by the California Institute of Technology, under contract with the National Aeronautics and Space Administration under the Exoplanet Exploration Program. This paper includes data collected by the *TESS* mission, which are publicly available from the Mikulski Archive for Space Telescopes (MAST). We thank Sam Kim, Régis Lachaume and Martin Schlecker for their technical assistance during the observations at the MPG 2.2 m Telescope

## REFERENCES

- Aguilera-Gómez, C., Chanamé, J., Pinsonneault, M. H., & Carlberg, J. K. 2016, *ApJ*, 829, 127
- Almenara, J. M., Damiani, C., Bouchy, F., et al. 2015, *A&A*, 575, A71
- Anderson, K. R., & Lai, D. 2017, *MNRAS*, 472, 3692
- Bakos, G., Noyes, R. W., Kovács, G., et al. 2004, *PASP*, 116, 266
- Bakos, G. Á., Csabry, Z., Penev, K., et al. 2013, *PASP*, 125, 154
- Baraffe, I., Homeier, D., Allard, F., & Chabrier, G. 2015, *A&A*, 577, A42
- Barclay, T., Pepper, J., & Quintana, E. V. 2018, *ArXiv e-prints*, arXiv:1804.05050

**Table 2.** Planetary properties of the HD 1397 system. For the priors,  $N(\mu, \sigma)$  stands for a normal distribution with mean  $\mu$  and standard deviation  $\sigma$ ,  $U(a, b)$  stands for a uniform distribution between  $a$  and  $b$ , and  $J(a, b)$  stands for a Jeffrey’s prior defined between  $a$  and  $b$ .

Parameter	Prior	Value
P (days)	$N(11.535, 0.001)$	$11.53508 \pm 0.00057$
$T_0$ (BJD)	$N(2458332.0816, 0.001)$	$2458332.08169 \pm 0.00046$
$a/R_\star$	$U(1, 300)$	$9.96^{+0.47}_{-0.47}$
b	$U(0, 1)$	$0.16^{+0.14}_{-0.11}$
$R_P/R_\star$	$U(0.01, 0.1)$	$0.04536^{+0.00035}_{-0.00026}$
$\sigma_w^{\text{TESS}}$ (ppm)	$J(1, 500)$	$6^{+16}_{-4}$
$q_1^{\text{TESS}}$	$U(0, 1)$	$0.146^{+0.036}_{-0.024}$
$q_2^{\text{TESS}}$	$U(0, 1)$	$0.85^{+0.10}_{-0.15}$
K (m s <sup>-1</sup> )	$U(0, 100)$	$26.1^{+1.3}_{-1.3}$
$\sqrt{e} \sin \omega$	$U(-1, 1)$	$0.096^{+0.086}_{-0.091}$
$\sqrt{e} \cos \omega$	$U(-1, 1)$	$0.435^{+0.029}_{-0.033}$
$\dot{\gamma}$ (m s <sup>-1</sup> / d)	$U(-10, 10)$	$0.38^{+0.07}_{-0.06}$
$\gamma_{\text{FEROS}}$ (m s <sup>-1</sup> )	$N(30755, 10)$	$30765.3^{+5.2}_{-4.3}$
$\gamma_{\text{HARPS}}$ (m s <sup>-1</sup> )	$N(30805, 10)$	$30804.4^{+5.1}_{-4.4}$
$\gamma_{\text{FIDEOS}}$ (m s <sup>-1</sup> )	$N(30699, 10)$	$30695.3^{+5.2}_{-4.7}$
$P^c$ (days)	$N(11.54, 0.01)$	$18.24 \pm 0.44$
$K^c$ (m s <sup>-1</sup> )	$N(0, 100)$	$7.5 \pm 1.4$
$T_0^c$ (BJD)	$N(2458323.5, 3)$	$2458323.67355 \pm 1.8$
$e$		$0.210 \pm 0.038$
$\omega$ (rad)		$0.19 \pm 0.20$
$i$ (deg)		$89.1 \pm 0.8$
$M_P$ (M <sub>J</sub> )		$0.335^{+0.018}_{-0.018}$
$R_P$ (R <sub>J</sub> )		$1.021^{+0.015}_{-0.014}$
$a$ (AU)		$0.10866^{+0.00037}_{-0.00045}$
$T_{\text{eq}}^a$ (K)		$1213 \pm 17$

<sup>a</sup>Time-averaged equilibrium temperature computed according to equation 16 of Méndez & Rivera-Valentín (2017)

- Bento, J., Hartman, J. D., Bakos, G. Á., et al. 2018, *MNRAS*, 477, 3406
- Bhatti, W., Bakos, G. Á., Hartman, J. D., et al. 2016, ArXiv e-prints, arXiv:1607.00322
- Bouchy, F., Udry, S., Mayor, M., et al. 2005, *A&A*, 444, L15
- Bowler, B. P., Johnson, J. A., Marcy, G. W., et al. 2010, *ApJ*, 709, 396
- Brahm, R., Jordán, A., & Espinoza, N. 2017a, *PASP*, 129, 034002
- Brahm, R., Jordán, A., Hartman, J., & Bakos, G. 2017b, *MNRAS*, 467, 971
- Brahm, R., Jordán, A., Bakos, G. Á., et al. 2016, *AJ*, 151, 89
- Brahm, R., Espinoza, N., Jordán, A., et al. 2018, *MNRAS*, 477, 2572
- Buchner, J., Georgakakis, A., Nandra, K., et al. 2014, *A&A*, 564, A125
- Castelli, F., & Kurucz, R. L. 2004, ArXiv e-prints, astro
- Chen, G., Pallé, E., Welbanks, L., et al. 2018, *A&A*, 616, A145
- Currie, T. 2009, *ApJL*, 694, L171
- Demory, B.-O., & Seager, S. 2011, *ApJS*, 197, 12
- Dong, S., Katz, B., & Socrates, A. 2014, *ApJL*, 781, L5
- Dunhill, A. C., Alexander, R. D., & Armitage, P. J. 2013, *MNRAS*, 428, 3072
- Espinoza, N., Brahm, R., Jordán, A., et al. 2016, *ApJ*, 830, 43
- Esposito, M., Covino, E., Desidera, S., et al. 2017, *A&A*, 601, A53
- Feroz, F., Hobson, M. P., & Bridges, M. 2009, *MNRAS*, 398, 1601
- Foreman-Mackey, D., Agol, E., Ambikasaran, S., & Angus, R. 2017, *AJ*, 154, 220
- Foreman-Mackey, D., Hogg, D. W., Lang, D., & Goodman, J. 2013, *PASP*, 125, 306
- Fortney, J. J., Marley, M. S., & Barnes, J. W. 2007, *ApJ*, 659, 1661
- Fulton, B. J., Petigura, E. A., Blunt, S., & Sinukoff, E. 2018, ArXiv e-prints, arXiv:1801.01947
- Gaia Collaboration, Brown, A. G. A., Vallenari, A., et al. 2018, ArXiv e-prints, arXiv:1804.09365
- Gaia Collaboration, Prusti, T., de Bruijne, J. H. J., et al. 2016, *A&A*, 595, A1
- Giuppone, C. A., Morais, M. H. M., & Correia, A. C. M. 2013, *MNRAS*, 436, 3547
- Grunblatt, S. K., Huber, D., Gaidos, E., et al. 2017, *AJ*, 154, 254
- Hartman, J. D., Bakos, G. Á., Béky, B., et al. 2012, *AJ*, 144, 139
- Hellier, C., Anderson, D. R., Collier Cameron, A., et al. 2015, *AJ*, 150, 18
- Hellier, C., Anderson, D. R., Cameron, A. C., et al. 2017, *MNRAS*, 465, 3693
- Henry, G. W., Marcy, G. W., Butler, R. P., & Vogt, S. S. 2000, *ApJL*, 529, L41
- Howell, S. B., Sobek, C., Haas, M., et al. 2014, *Publications of the Astronomical Society of the Pacific*, 126, 398
- Hussain, G. A. J. 2002, *Astronomische Nachrichten*, 323, 349
- Jenkins, J. S., Jones, H. R. A., Pavlenko, Y., et al. 2008, *A&A*, 485, 571
- Jensen, A. G., Cauley, P. W., Redfield, S., Cochran, W. D., & Endl, M. 2018, *AJ*, 156, 154
- Johnson, J. A., Howard, A. W., Bowler, B. P., et al. 2010, *PASP*, 122, 701
- Jones, M. I., Brahm, R., Wittenmyer, R. A., et al. 2017, *A&A*, 602, A58
- Jones, M. I., Jenkins, J. S., Bluhm, P., Rojo, P., & Melo, C. H. F. 2014, *A&A*, 566, A113
- Jones, M. I., Brahm, R., Espinoza, N., et al. 2018, *A&A*, 613, A76
- Jordán, A., Brahm, R., Espinoza, N., et al. 2018, ArXiv e-prints, arXiv:1809.08879
- Kaufer, A., Stahl, O., Tubbesing, S., et al. 1999, *The Messenger*, 95, 8
- Kempton, E. M.-R., Bean, J. L., Louie, D. R., et al. 2018, ArXiv e-prints, arXiv:1805.03671
- Kipping, D. M. 2013, *MNRAS*, 435, 2152
- Knutson, H. A., Fulton, B. J., Montet, B. T., et al. 2014, *ApJ*, 785, 126
- Kovács, G., Bakos, G. Á., Hartman, J. D., et al. 2010, *ApJ*, 724, 866
- Kozai, Y. 1962, *AJ*, 67, 591
- Kreidberg, L. 2015, *PASP*, 127, 1161
- Lendl, M., Triaud, A. H. M. J., Anderson, D. R., et al. 2014, *A&A*, 568, A81
- Lendl, M., Anderson, D. R., Bonfanti, A., et al. 2018, *MNRAS*, arXiv:1807.06973
- Lidov, M. L. 1962, *Planet. Space Sci.*, 9, 719
- Lopez, E. D., & Fortney, J. J. 2016, *ApJ*, 818, 4
- Mayor, M., Pepe, F., Queloz, D., et al. 2003, *The Messenger*, 114, 20
- Méndez, A., & Rivera-Valentín, E. G. 2017, *ApJL*, 837, L1
- Naoz, S. 2016, *ARA&A*, 54, 441
- Pepper, J., Pogge, R. W., DePoy, D. L., et al. 2007, *PASP*, 119, 923
- Pepper, J., Rodriguez, J. E., Collins, K. A., et al. 2017, *AJ*, 153, 215

- Petrovich, C., & Tremaine, S. 2016, *ApJ*, 829, 132
- Petrovich, C., Tremaine, S., & Rafikov, R. 2014, *ApJ*, 786, 101
- Pollacco, D. L., Skillen, I., Collier Cameron, A., et al. 2006, *PASP*, 118, 1407
- Pollack, J. B., Hubickyj, O., Bodenheimer, P., et al. 1996, *Icarus*, 124, 62
- Rabus, M., Jordán, A., Hartman, J. D., et al. 2016, *AJ*, 152, 88
- Ricker, G. R., Winn, J. N., Vanderspek, R., et al. 2015, *Journal of Astronomical Telescopes, Instruments, and Systems*, 1, 014003
- Schlaufman, K. C., & Winn, J. N. 2013, *ApJ*, 772, 143
- Shporer, A., Zhou, G., Fulton, B. J., et al. 2017, *AJ*, 154, 188
- Smith, A. M. S., Anderson, D. R., Bouchy, F., et al. 2013, *A&A*, 552, A120
- Smith, A. M. S., Gandolfi, D., Barragán, O., et al. 2017, *MNRAS*, 464, 2708
- Spake, J. J., Sing, D. K., Evans, T. M., et al. 2018, *Nature*, 557, 68
- Talens, G. J. J., Spronck, J. F. P., Lesage, A.-L., et al. 2017, *A&A*, 601, A11
- Triaud, A. H. M. J., Collier Cameron, A., Queloz, D., et al. 2010, *A&A*, 524, A25
- Van Eylen, V., Albrecht, S., Gandolfi, D., et al. 2016, *AJ*, 152, 143
- Vanzi, L., Zapata, A., Flores, M., et al. 2018, *ArXiv e-prints*, arXiv:1804.07441
- Villaver, E., & Livio, M. 2009, *ApJL*, 705, L81
- Villaver, E., Livio, M., Mustill, A. J., & Siess, L. 2014, *ApJ*, 794, 3
- Wang, S., Jones, M., Shporer, A., et al. 2018, *ArXiv e-prints*, arXiv:1810.02341
- Welsh, W. F., Orosz, J. A., Seager, S., et al. 2010, *The Astrophysical Journal Letters*, 713, L145.  
<http://stacks.iop.org/2041-8205/713/i=2/a=L145>
- Yi, S., Demarque, P., Kim, Y.-C., et al. 2001, *ApJS*, 136, 417
- Yu, L., Rodriguez, J. E., Eastman, J. D., et al. 2018, *ArXiv e-prints*, arXiv:1803.02858
- Zechmeister, M., & Kürster, M. 2009, *A&A*, 496, 577
- Zhou, G., Bayliss, D., Hartman, J. D., et al. 2015, *ApJL*, 814, L16

## APPENDIX

**Table 3.** Relative radial velocities and bisector spans for HD 1397.

BJD (2,400,000+)	RV (km s <sup>-1</sup> )	$\sigma_{RV}$ (km s <sup>-1</sup> )	BIS (km s <sup>-1</sup> )	$\sigma_{BIS}$ (km s <sup>-1</sup> )	S index	$\sigma_{Sindex}$	Instrument
2458367.68314629	30.7863	0.0020	0.022	0.002	.....	.....	HARPS
2458368.66398162	30.7806	0.0020	0.021	0.002	.....	.....	HARPS
2458368.68745551	30.6687	0.0066	-0.013	0.006	.....	.....	FIDEOS
2458368.69912355	30.6521	0.0066	-0.028	0.006	.....	.....	FIDEOS
2458368.70678972	30.6834	0.0073	0.002	0.007	.....	.....	FIDEOS
2458368.75311381	30.6773	0.0068	-0.032	0.007	.....	.....	FIDEOS
2458368.76041725	30.6538	0.0071	-0.022	0.007	.....	.....	FIDEOS
2458368.85411697	30.6615	0.0081	-0.011	0.009	.....	.....	FIDEOS
2458368.86145728	30.6624	0.0080	-0.034	0.008	.....	.....	FIDEOS
2458369.64418781	30.6956	0.0071	-0.038	0.007	.....	.....	FIDEOS
2458369.65198892	30.6926	0.0072	-0.008	0.007	.....	.....	FIDEOS
2458369.65923657	30.6669	0.0071	-0.037	0.007	.....	.....	FIDEOS
2458369.78679607	30.6421	0.0075	-0.036	0.008	.....	.....	FIDEOS
2458369.79512629	30.6764	0.0077	-0.014	0.008	.....	.....	FIDEOS
2458369.80270826	30.6555	0.0076	-0.029	0.008	.....	.....	FIDEOS
2458370.64460774	30.6861	0.0068	0.006	0.007	.....	.....	FIDEOS
2458370.65242178	30.6809	0.0067	0.003	0.007	.....	.....	FIDEOS
2458370.66037165	30.6822	0.0068	0.005	0.007	.....	.....	FIDEOS
2458370.78118598	30.6629	0.0079	-0.008	0.008	.....	.....	FIDEOS
2458370.78842912	30.6683	0.0078	-0.016	0.008	.....	.....	FIDEOS
2458370.79561044	30.6631	0.0079	0.005	0.008	.....	.....	FIDEOS
2458371.64189723	30.6767	0.0078	-0.026	0.008	.....	.....	FIDEOS
2458371.64982610	30.6960	0.0079	-0.044	0.008	.....	.....	FIDEOS
2458371.65723468	30.6510	0.0137	0.025	0.014	.....	.....	FIDEOS
2458371.77405182	30.6681	0.0078	-0.005	0.008	.....	.....	FIDEOS
2458371.78144230	30.6848	0.0078	-0.009	0.008	.....	.....	FIDEOS
2458371.78862670	30.6807	0.0075	-0.019	0.008	.....	.....	FIDEOS
2458371.87779688	30.6601	0.0095	0.011	0.010	.....	.....	FIDEOS
2458372.65137095	30.6693	0.0067	0.002	0.007	.....	.....	FIDEOS
2458372.65854816	30.6858	0.0069	-0.018	0.007	.....	.....	FIDEOS
2458372.67407844	30.6880	0.0067	-0.014	0.007	.....	.....	FIDEOS
2458372.79013200	30.7100	0.0083	0.017	0.009	.....	.....	FIDEOS
2458372.79735118	30.6948	0.0082	0.005	0.009	.....	.....	FIDEOS
2458372.80462143	30.6821	0.0083	0.001	0.009	.....	.....	FIDEOS
2458373.75687607	30.7194	0.0088	0.051	0.009	.....	.....	FIDEOS
2458373.76411946	30.7301	0.0088	0.015	0.009	.....	.....	FIDEOS
2458379.71952476	30.7427	0.0050	0.001	0.003	0.1963	0.0019	FEROS
2458379.72709860	30.7462	0.0050	0.002	0.003	0.1942	0.0018	FEROS
2458379.73465009	30.7490	0.0050	0.001	0.003	0.1923	0.0019	FEROS
2458383.71877730	30.7464	0.0050	0.004	0.003	0.1905	0.0018	FEROS
2458383.72286419	30.7444	0.0050	0.002	0.003	0.1941	0.0018	FEROS
2458383.72928826	30.7401	0.0050	0.001	0.003	0.2323	0.0021	FEROS
2458384.74720465	30.7524	0.0050	0.005	0.003	0.1940	0.0019	FEROS
2458384.75128807	30.7588	0.0050	0.006	0.003	0.1947	0.0019	FEROS

2458384.75537333	30.7585	0.0050	0.002	0.003	0.1933	0.0020	FEROS
2458385.69639408	30.7720	0.0050	0.001	0.003	0.1890	0.0017	FEROS
2458385.70045388	30.7691	0.0050	0.000	0.003	0.1851	0.0018	FEROS
2458385.70451623	30.7669	0.0050	0.001	0.003	0.1935	0.0017	FEROS
2458398.85664355	30.7997	0.0050	-0.002	0.003	0.1852	0.0030	FEROS
2458398.86160055	30.7927	0.0050	-0.002	0.003	0.1991	0.0038	FEROS
2458398.86646831	30.8011	0.0050	0.006	0.003	0.1789	0.0037	FEROS
2458401.67766910	30.7623	0.0050	0.002	0.003	0.2000	0.0018	FEROS
2458401.68490538	30.7610	0.0050	0.000	0.003	0.1980	0.0017	FEROS
2458401.68884631	30.7641	0.0050	0.006	0.003	0.1973	0.0018	FEROS
2458404.50796278	30.7509	0.0050	0.006	0.003	0.1955	0.0028	FEROS
2458406.54669111	30.7631	0.0050	0.006	0.003	0.2147	0.0025	FEROS
2458406.55379532	30.7593	0.0050	0.005	0.003	0.2109	0.0025	FEROS
2458406.55921117	30.7620	0.0050	0.002	0.003	0.2151	0.0025	FEROS
2458407.51309835	30.7715	0.0050	0.008	0.003	0.2121	0.0026	FEROS
2458407.51829310	30.7741	0.0050	0.004	0.003	0.2008	0.0034	FEROS
2458407.52382158	30.7766	0.0050	0.015	0.003	0.2121	0.0035	FEROS
2458409.61580549	30.8010	0.0050	0.008	0.003	0.2164	0.0020	FEROS
2458409.62127285	30.8011	0.0050	0.003	0.003	0.2168	0.0020	FEROS
2458410.69117440	30.8143	0.0050	0.003	0.003	0.2107	0.0024	FEROS
2458411.68527663	30.8072	0.0050	0.002	0.003	0.2167	0.0020	FEROS
2458411.68936375	30.8089	0.0050	0.005	0.003	0.2136	0.0020	FEROS
2458411.69344901	30.8056	0.0050	0.009	0.003	0.2176	0.0021	FEROS
2458412.65419276	30.7916	0.0050	0.003	0.003	0.2101	0.0016	FEROS
2458412.65825916	30.7853	0.0050	0.004	0.003	0.2110	0.0017	FEROS
2458412.66232846	30.7872	0.0050	0.003	0.003	0.2101	0.0017	FEROS
2458413.56187674	30.7734	0.0050	0.005	0.003	0.2067	0.0015	FEROS
2458413.56594013	30.7713	0.0050	0.004	0.003	0.2101	0.0016	FEROS
2458413.57000699	30.7723	0.0050	0.003	0.003	0.2073	0.0017	FEROS
2458414.64539175	30.7621	0.0050	0.006	0.006	0.2081	0.0019	FEROS
2458414.64946278	30.7646	0.0050	0.007	0.006	0.2079	0.0017	FEROS
2458414.65458118	30.7597	0.0050	0.003	0.006	0.2087	0.0018	FEROS
2458415.63730889	30.7569	0.0050	0.004	0.007	0.2119	0.0020	FEROS
2458415.64138930	30.7544	0.0050	0.004	0.006	0.2046	0.0020	FEROS
2458415.64547434	30.7619	0.0050	0.005	0.007	0.2072	0.0021	FEROS
2458416.60613278	30.7547	0.0050	0.002	0.006	0.2076	0.0016	FEROS
2458416.61019593	30.7487	0.0050	0.003	0.006	0.2059	0.0017	FEROS
2458416.61426082	30.7570	0.0050	0.004	0.006	0.2040	0.0016	FEROS
2458417.52542561	30.7916	0.0020	0.023	0.002	.....	.....	HARPS
2458418.61188680	30.7580	0.0050	0.005	0.006	0.20121	0.0015541	FEROS
2458418.61596421	30.7608	0.0050	0.004	0.006	0.20046	0.0016165	FEROS
2458418.62002979	30.7593	0.0050	0.007	0.006	0.19964	0.0016737	FEROS
2458419.58562321	30.7659	0.0050	0.005	0.006	0.20384	0.0017164	FEROS
2458419.58968614	30.7663	0.0050	0.001	0.006	0.20433	0.0017265	FEROS
2458419.58156051	30.7685	0.0050	0.001	0.006	0.20151	0.0016520	FEROS
2458419.64824552	30.8056	0.0020	0.023	0.002	.....	.....	HARPS